J. Fluid Mech. (1972), *vol.* 54, *part* 4, *pp.* 613–625
Printed in Great Britain

An electrochemical study of flow instability on a rotating disk

By DER-TAU CHIN† AND MITCHELL LITT
School of Chemical Engineering, University of Pennsylvania, Philadelphia

(Received 11 March 1970 and in revised form 5 January 1972)

Data for the fluctuating mass-transfer coefficient to point electrodes on the surface of a rotating disk are presented for transition and turbulent flow, along with analysis of the energy spectrum. The results corroborate previous evidence of standing vortices on the surface in the transition region. It is shown that the electrochemical method gives a more sensitive probe of flow instabilities than has been possible previously; the transition region is found to be wider than has been previously thought to be and lies between roughly $Re = 1{\cdot}7 \times 10^5$ and $3{\cdot}5 \times 10^5$, where $Re = r^2\omega/\nu$ is the Reynolds number, ω being the angular velocity of the disk (in rad/s) and ν the kinematic viscosity. As the Reynolds number is increased, the stationary vortices in the transition region propagate primarily with a frequency matching that of the disk speed. After a peak energy has been reached at $Re = 2{\cdot}6 \times 10^5$, the vortices break down into a fully developed turbulent flow.

1. Introduction and background

In a previous paper (Chin & Litt 1972) we have presented a theory and an experimental technique that were used to study mass transfer from isolated point electrodes on the surface of a rotating disk. Since, on a rotating disk, the laminar, transition and turbulent régimes can exist simultaneously at different radii, such a system is most useful in studying flow instability and transition to turbulent flow. Also, the rotating disk, giving rise to a three-dimensional flow system, offers a possibility of studying instability in the three-dimensional flow field. This paper presents the results of a preliminary study of the transition régime on a rotating disk, using the polarized point-electrode technique described earlier.

The principal use of the rotating disk geometry has been in laminar flow, for which, as the Levich (1962) theory shows, the diffusion field is one-dimensional. However, this is not true in turbulent flow. Several workers (Serad 1964; Kreith, Taylor & Chong 1959), who performed mass-transfer experiments on rotating disks of suitable size, have reported spiral patterns on the outer region of the disk surface. The spirals did not originate at the centre of the disk, but at a radius dependent upon the rotational speed. It is evident that these patterns are a visual

† Present address: Electrochemistry Department, Research Laboratories, General Motors Corporation, Warren, Michigan 48090.

indication of the radial position where flow instabilities begin. For this reason, and because the rotating disk is a model three-dimensional flow field, there have been a number of studies of flow instability on the rotating disk.

Smith (1947), using a hot-wire probe on a well-polished steel disk, observed sinusoidal waves excited by random disturbances to begin at a Reynolds number of $2{\cdot}1 \times 10^5$. The direction of the waves makes an angle of about 14° with the outward radius vector. Gregory, Stuart & Walker (1955) employed a wet china-clay-coated disk rotating in stationary air at a constant temperature. Since the mass-transfer rate is higher in turbulent than in laminar flow, after a certain period of rotation the turbulent areas of the disk dried completely, while the laminar areas were still wet. They observed two critical radii separating three different flow regions on the disk surface. Within the inner radius the flow was purely laminar, and beyond the outer radius completely turbulent. Between the two radii was the area of transition where a series of traces in the form of equi-angular spirals were found. The spiral path was inclined at about 14° to the tangential direction and coincided well with Smith's observation. They attributed such traces to the presence of stationary vortices in the boundary layer. Regarding the inner radius as the position of onset of instability and the outer one as the point of transition to turbulence, they obtained an instability Reynolds number of $1{\cdot}9 \times 10^5$ and a transition Reynolds number of $2{\cdot}9 \times 10^5$. The approximate number of vortices observed on the surface was between 28 and 31. In a later study (Gregory & Walker 1960) of the effect of suction through a slitted disk, these authors further demonstrated that the transition boundary layer was composed of a vortex régime and an intermediate turbulent régime.

Stuart's analysis (Gregory *et al.* 1955) showed that, for inviscid rotating disk flow, the stationary vortices should propagate at an angle of $13\frac{1}{4}°$ to the tangential vector, in good agreement with the experimental observations. However, the calculated wavenumbers varied between 113 and 140, being about four times greater than the experimental values. This discrepancy he ascribed to the neglect of viscosity. The stability problem was later solved numerically by Brown (1961), who computed neutral stability curves for both the cross-flow and the critical-flow profiles. The point of instability was found to be at $Re = 3{\cdot}2 \times 10^4$, which was considerably lower than the experimental value. More recently, Cham & Head (1969) studied the development of the turbulent boundary layer on a disk rotating in air. Their results basically confirm those of Gregory *et al.* (1955), and further demonstrate that the turbulent boundary layer can be treated as a function of the Reynolds number based on the disk radius alone.

Faller & Kaylor (1966), using the Ekman boundary layer as an analogy, performed a visual investigation on flow instability on the rotating disk. The stationary vortex was found to have a wavelength of $22(\nu/\omega)^{\frac{1}{2}}$. In addition to the stationary vortex, they also detected a parallel instability for which the Coriolis forces played an important role. This different type of vortex had a wavelength of approximately $44(\nu/\omega)^{\frac{1}{2}}$ and differed from the stationary one in that it occurred sporadically with rapid movement.

In the fully developed turbulent boundary layer, non-stationary vortex

phenomena, which the china-clay technique had failed to detect, were later reported by Kreith *et al.* (1959), who studied sublimation of a naphthalene disk in air. The spiral vortices were visible not only in the transitional region, but also in the fully developed turbulent region. The scales of the turbulent vortices appeared to be much smaller than in the transition region. This fact suggests that the vortices may remain attached to the disk surface even in the viscous sublayer.

On the other hand, it seems surprising that there have been repeated reports, from investigators studying metal deposition and dissolution reactions (Gregory & Riddiford 1960; Johnson & Turner 1962; Rogers & Taylor 1963*a*, *b*), of imprinted spiral traces in the laminar region. These traces are displaced from the centre of the disk in an equi-angular direction making an angle of about 30° with the outward radius vector. Although the disk was non-uniform in appearance, the overall rate of mass transfer to the disk was still in good agreement with the Levich theory. It appears, therefore, that in spite of the uniform flow there may exist localized disturbances even within the laminar boundary layer. Such disturbances, as explained by Rogers & Taylor (1963*a*), may be caused by small protrusions, such as burrs or gas bubbles attached on the surface.

With this background, it appears to us that the polarized point-electrode technique (Reiss & Hanratty 1962, 1963; Mitchell & Hanratty 1966) would be an ideal experimental tool for studying instability in the rotating disk system. Since the electrodes are mounted flush with the surface they do not interfere with the flow. Because the limiting current measures the instantaneous rate of mass transfer to the electrodes, which are smaller than the scale of turbulence, the fluctuations in the limiting current should reflect the instability in the flow field. For a system with large Schmidt number, the concentration boundary layer is well within the momentum boundary layer so these fluctuations can be attributed to the flow field rather than the concentration field variations. Also, by varying the shape and location of the point electrodes, it should be possible to study particular features of the flow structure. In particular, since the electrode is stationary relative to the surface, such an electrode is ideal for studying the stationary surface vortices.

2. Experiments

Three types of surface-mounted point electrodes are used in this study: (i) a local probe, which is either a 0·0254 cm or a 0·0381 cm diameter circular platinum electrode mounted flush on the disk surface; (ii) a radial probe, which is a rectangular platinum electrode, 0·003 cm wide by 0·254 cm long, mounted parallel to the tangential direction; (iii) a tangential probe, also a 0·003 cm by 0·254 cm platinum electrode mounted parallel to the radial direction. The details of the experimental set up have been given previously (Chin 1969; Chin & Litt 1972) and will not be repeated here. For the present study, however, separate electronics are used to determine the root mean square of the limiting current fluctuations as well as the time-averaged current. Since we have

$$I_l = \bar{I}_l + i_l = KAnFC_\infty,$$

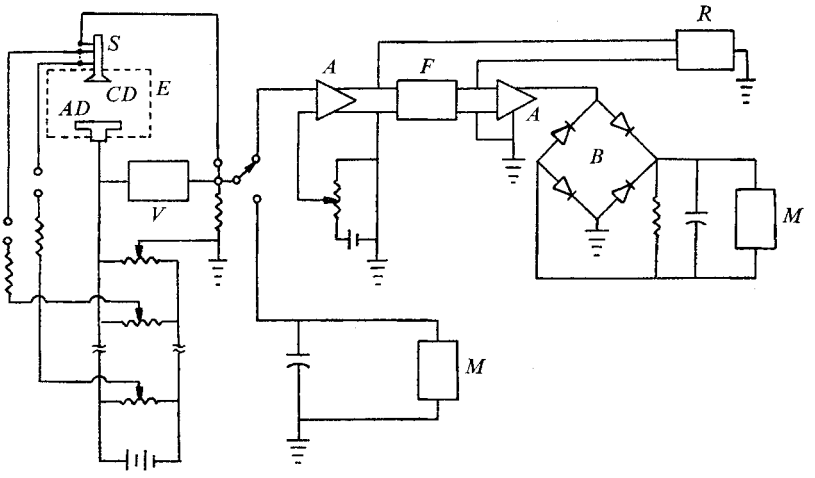

FIGURE 1. Electrical circuit. A, differential amplifier; AD, anode; B, rectifying bridge; CD, cathodic point-electrodes on the surface of a Lucite rotating disk; E, electrolytic cell; F, ultra-low-frequency filter; M, microvoltmeter; R, recorder; S, slip-ring contacts; V, solid-state voltmeter.

where I_l is the limiting current, i_l is the fluctuating part of I_l, K is the mass-transfer coefficient, F the Faraday constant, A the surface area of the point electrodes, n the number of electrons transferred in electrode reactions, C_∞ the bulk concentration of the diffusing ion, and an over bar indicates a time average, K can also be separated into a time-averaged component and a fluctuation

$$K = \bar{K} + k.$$

Thus, the fluctuation mass transfer coefficient k is related to the measured limiting current fluctuation by

$$k = i_l / AnFC_\infty$$

and

$$(\overline{k^2})^{\frac{1}{2}}/\bar{K} = (\overline{i_l^2})^{\frac{1}{2}}/\bar{I}_l.$$

A spectrum function $E(\tilde{\omega})$ is defined such that $E(\tilde{\omega})\,d\tilde{\omega}$ is the contribution to $\overline{k^2}/\bar{K}^2$ of the wave frequencies between $\tilde{\omega}$ and $\tilde{\omega}+d\tilde{\omega}$ (Hinze 1959). The spectrum function must satisfy the condition

$$\frac{\overline{k^2}}{\bar{K}^2} = \int_0^\infty E(\tilde{\omega})\,d\tilde{\omega}.$$

The electric circuit used to measure the current fluctuations is shown in figure 1. The d.c. input to the circuit is supplied by a 6 V battery. The applied potential drop across the cell is controlled by a 350 ohm potentiometer and is measured by a solid-state voltmeter (Heathkit IM-17). The limiting current is obtained by measuring the voltage drop across a 1000-ohm standard resistor. A d.c. microvoltmeter (Keithley 151) with a 10000 MF capacitor connected across the two terminals is used to measure the time-averaged component. The current fluctuation is measured by feeding the signal to a differential amplifier (Sanborn 8875 A), the d.c. component of the signal being eliminated by supplying

a d.c. signal to the second input terminal of the amplifier. The fluctuating output from the amplifier is then sent to an ultra-low-frequency band-pass filter (Krohn-Hite 330A), which is used for two purposes: to eliminate completely the d.c. component and for spectrum analysis. Both the input and the output of the band-pass filter are sent to a recorder (Brush Mark II) for visual examination. The output from the band-pass filter is fed to a second differential amplifier. The root mean square of the fluctuating component is finally measured by feeding the signal to a rectifying bridge and measuring the d.c. voltage drop across a 109-ohm load resistor and a 190000 MF capacitor with a d.c. microvoltmeter (Keithley 151). The bridge rectifier is composed of four germanium diodes, types 1N 99. The d.c. voltage drop across the load resistor has been calibrated against the r.m.s. voltage of a signal generator used as the input signal. It is found that the d.c. voltage from the rectifying bridge is relatively independent of the frequency of the a.c. input. The reason that the r.m.s. voltage is measured by rectifying the signal instead of using a true r.m.s. voltmeter is that the fluctuating signal is modulated by a very low-frequency component (about 0·5 c/s) of large amplitude, which makes it difficult to take a reading even on a true r.m.s. voltmeter (such as Ballantine 320) because the meter needle fluctuates with this frequency. With the fairly large time constant provided by the load resistor and the large capacitor, it has been possible to measure the r.m.s. voltage of the a.c. signal down to 0.3 c/s with an accuracy of 95 %. The entire electrolytic cell is shielded by a Faraday cage made of aluminium screening, which greatly reduces electric noise level. All the measurements are made at a room temperature of 22 ± 2 °C.

3. Results and discussion

Intensity of fluctuations

The results for a 0·0381 cm diameter local probe are presented in figure 2, where the mass fluctuation intensity $(\overline{k^2})^{\frac{1}{2}}/\overline{K}$ is plotted against the rotational speed for various radial positions. These curves are typical of the data obtained, so the raw data with the other probes are not shown here (but are reported in Chin 1969).

Figure 2 shows that each probe gives a distinct curve. As the disk speed is increased energy appears in the fluctuating components, first for larger radii and then for inner radii. Each curve seems to possess a distinct peak energy, which soon drops to a uniform level with increasing speed of rotation. The speed at which the peak intensity occurs depends upon the radial position: the larger the radius, the lower the speed. These results have been further checked by measuring the fluctuating limiting current directly with a Greibach true r.m.s. milliammeter rather than the rectifier bridge, and the same behaviour was observed. This proves that the peak is not an artifact caused by the element of the measuring circuit, but a direct result of the interaction of vortices near the disk surface.

These curves are re-plotted against Reynolds number in figure 3; also included in the figure are the data obtained with the smaller size local probes. On this basis, the individual peaks seem to have been brought together and occur at a single Reynolds number of $2{\cdot}6 \times 10^5$. It is seen that, on the basis of the fluctuating

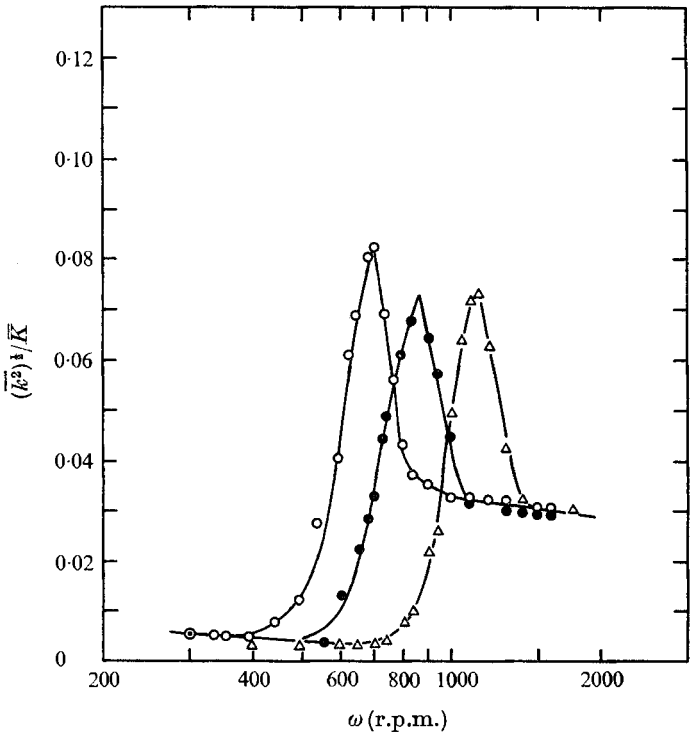

FIGURE 2. Fluctuating mass flux to a 0·0381 cm diameter local probe. ○, r = 6·01 cm; ●, r = 5·40 cm; △, r = 4·77 cm.

data, the transition region is actually wider than it has previously been thought to be. Energy appears in the fluctuating components at a Reynolds number as low as $1{\cdot}7 \times 10^5$, and does not become essentially constant until a value of $3{\cdot}5 \times 10^5$ is reached. In a previous paper (Chin & Litt 1972) we have shown that, based on the values of the time-averaged mass-transfer coefficient, the transition region lay between 2·3 and $3{\cdot}0 \times 10^5$. Table 1 summarizes the values of the critical Reynolds numbers that have previously been reported, using various techniques. It is seen that the agreement between the time-averaged transfer data and those of the other techniques is good. The ability of the electrochemical method to follow the limiting current fluctuations, however, gives a more sensitive probe of the instability of flow than has been possible previously, particularly at the low-speed end of the transition region.

Structure of the transition boundary layer

Some insight into the transition phenomena occurring here can be gained by recalling the china-clay technique of Gregory *et al.* (1955), which indicates that standing vortices are set up in the transition region. In a later study using a slitted rotating disk Gregory & Walker (1960) further demonstrate that the transition region is composed of two subrégimes: (i) a vortex region and (ii) an intermediate turbulent region. Their data over the slitted surface at zero suction give $Re = 1{\cdot}3$–$2{\cdot}5 \times 10^5$ for the vortex region and $Re = 2{\cdot}5$–$2{\cdot}8 \times 10^5$ for

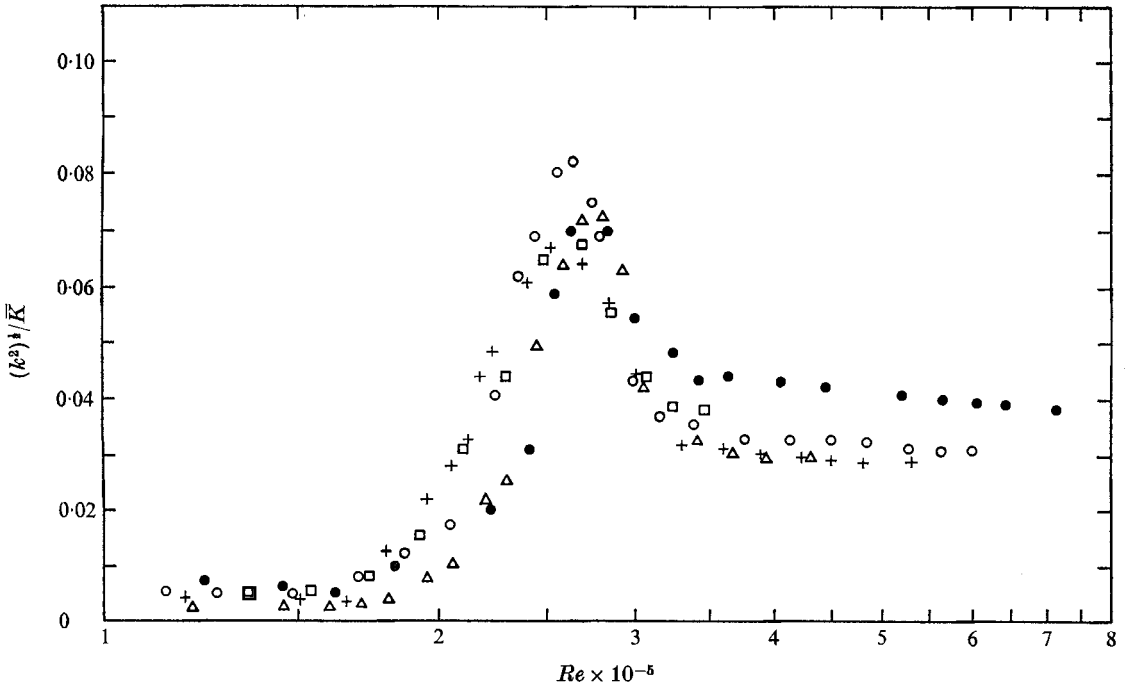

FIGURE 3. Fluctuation intensity *vs.* Reynolds numbers for the local probe. d = probe diameter.

	○	+	△	●	□
d (cm)	0·0381	0·0381	0·0381	0·0254	0·0254
r (cm)	6·01	5·40	4·77	6·03	4·13

Investigator	Technique	Point of instability	Point of transition
Schmidt (1921)	Turning moment coefficient	—	2×10^5
Kempf (1924)	Turning moment coefficient	—	7×10^4
Theodorsen & Regier (1944)	Turning moment coefficient	—	$3{\cdot}1 \times 10^5$
Smith (1947)	Hot-wire probe	$2{\cdot}1 \times 10^5$	—
Gregory, Stuart & Walker (1955)	China-clay method	$1{\cdot}9 \times 10^5$	$2{\cdot}9 \times 10^5$
Cobb & Saunders (1956)	Heat transfer from the disk	$2{\cdot}0 \times 10^5$	$2{\cdot}4 \times 10^5$
Kreith, Taylor & Chong (1959)	Mass transfer from the disk	$2{\cdot}1 \times 10^5$	—
Present authors	Point electrode, mean mass flux	$2{\cdot}3 \times 10^5$	$3{\cdot}0 \times 10^5$
Present authors	Point electrode, fluctuating mass flux	$1{\cdot}7 \times 10^5$	$3{\cdot}5 \times 10^5$

TABLE 1. Critical Reynolds numbers

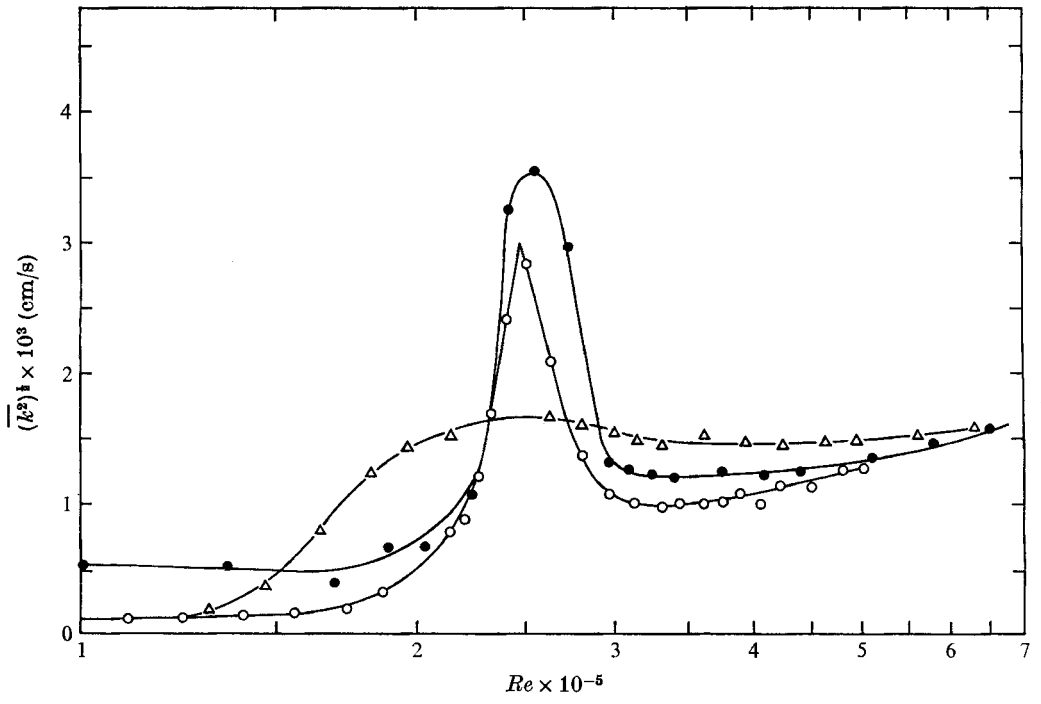

FIGURE 4. Comparison of mass-transfer fluctuations for a local, radial, and tangential probe. ○, $r = 5{\cdot}40$ cm, local probe; △, $r = 5{\cdot}55$ cm, radial probe; ●, $r = 5{\cdot}55$ cm, tangential probe.

the intermediate turbulent region. It appears that in the transition region the fluctuation in the limiting current is caused by a periodic flow component within the standing vortex. The region to the left of the peak in figure 3 ($1{\cdot}7 \times 10^5 < Re < 2{\cdot}6 \times 10^5$) represents the vortex region for a smooth disk, where the stationary vortices are amplified or growing in amplitude. Beyond the peak point is the intermediate turbulent region

$$(2{\cdot}6 \times 10^5 < Re < 3{\cdot}5 \times 10^5),$$

where the stationary vortices are breaking down into smaller size eddies as the region of the fully developed turbulence is approached. The behaviour of the fluctuation data beyond $Re = 3{\cdot}5 \times 10^5$ indicates that stable eddies have been formed. In the turbulent region, the intensity of the fluctuating mass flux becomes independent of Reynolds number. This result is similar to that found by Mitchell & Hanratty (1966) for pipe flow, although the absolute level of the intensity is about one-half of that from the pipe flow data.

Behaviour of the radial and the tangential probes

For comparison, the root mean square of the fluctuation mass-transfer coefficient of a local, a radial and a tangential probe, located at approximately the same radius, are plotted against Reynolds number in figure 4. It is seen that for the local and the tangential probes the curve exhibits a sharp and distinct peak energy, which occurs at $Re = 2{\cdot}6 \times 10^5$. The behaviour of the radial probe provides

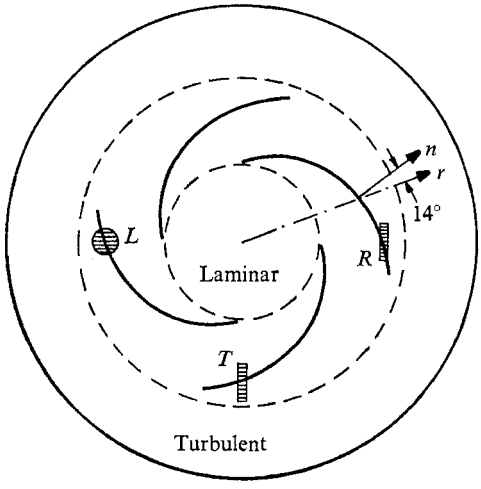

FIGURE 5. Stationary vortices and three types of point-electrodes. L, local probe; n, direction normal to the stationary vortex; r, radial direction; R, radial probe; T, tangential probe.

a further evidence that the fluctuation peak is directly related to the stationary vortex in the transition region. The direction normal to the propagation of the stationary vortices as measured by Smith (1947) and Gregory *et al.* (1955) is 14° to the outward radius vector. In other words, the direction of propagation makes an angle of 76° with the radial direction. The shape of the stationary vortices and their relations to the three kinds of point electrodes are illustrated in figure 5. It is seen that the vortex is almost in phase with the radial probe. The vortex size, as calculated from the results of Faller & Kaylor (1966), is approximately 0·2 cm, using $\nu = 0{\cdot}01$ cm^2/s and $\omega = 100$ rad/s, which corresponds to the typical conditions in our experiments. The long dimension of the radial probe is 0·254 cm, so there is considerable spatial averaging for the radial probe. This greatly reduces the ability of the radial probe to detect the fluctuating mass flux caused by the stationary vortex, whereas these fluctuations do show up for the tangential and the local probes.

Spectral analysis

In observing oscillographs of the fluctuating mass flux, a number of interesting phenomena have been noted. Frequencies corresponding to the disk speed tend to be amplified in the vortex region. As the disk speed is raised, new frequencies appear in the waves, which grow more intense, and then decrease sharply beyond the Reynolds number of peak intensity. The frequency of the waves, however increases with increasing rotational speed, and becomes much higher than the disk frequency in the intermediate and the turbulent regions. In an attempt to explore this further, spectral analysis has been undertaken for the fluctuating components of all three different probes. The results for the 0·0381 cm diameter local probe are given in figures 6–8. Again, these are the typical of the data obtained, so the spectral data for the other probes are not shown here.

Figure 6 gives the frequency spectrum for a local probe located at $r = 6{\cdot}01$ cm

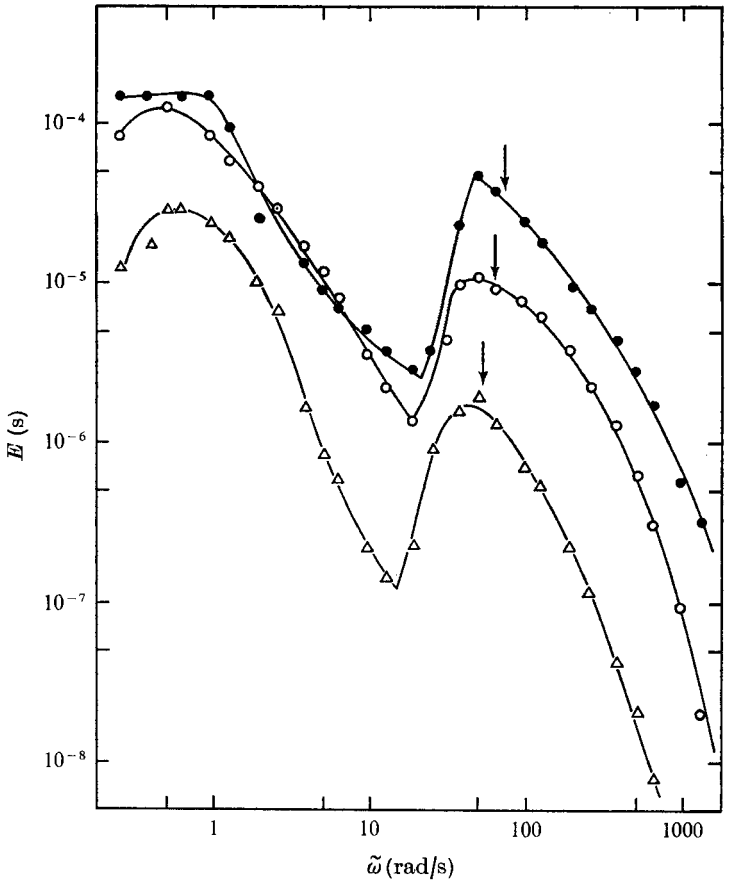

FIGURE 6. Frequency spectrum of a 0·0381 cm diameter local probe in the vortex region. The probe is located at $r = 6{\cdot}01$ cm. The disk speed ω in rad/s is indicated by the arrows. △, $\omega = 52$ rad/s, $Re = 1{\cdot}88 \times 10^5$; ○, $\omega = 62{\cdot}6$ rad/s, $Re = 2{\cdot}24 \times 10^5$; ●, $\omega = 73{\cdot}5$ rad/s, $Re = 2{\cdot}68 \times 10^5$.

in the vortex region. On each curve, the arrow represents the rotational frequency of the disk, in rad/s. The energy is highest at low frequencies, decreases with increasing frequency and then peaks at a frequency corresponding to the disk speed. The energy level increases with the disk speed, and reaches its maximum at a speed of 7·35 rad/s, which corresponds to the peak Reynolds number in figure 3. One might think that instabilities could perhaps arise from a mechanical cause, such as oscillation of the disk. That this is not an artifact of the measurement technique is shown in figure 7, where the spectra of the same probe obtained in the intermediate turbulent region are plotted. It is seen again that the energy maximum is at 73·5 rad/s. In this case, however, the lowest curve corresponds to a speed in the fully developed turbulent region. There is no evidence of amplification of the disk frequency for this curve; such amplification would be expected if some oscillation of the disk were giving rise to this phenomenon.

Figure 8 gives the spectral data from two local probes located at different radial positions when the disk is rotating at 120 rad/s. At this particular speed,

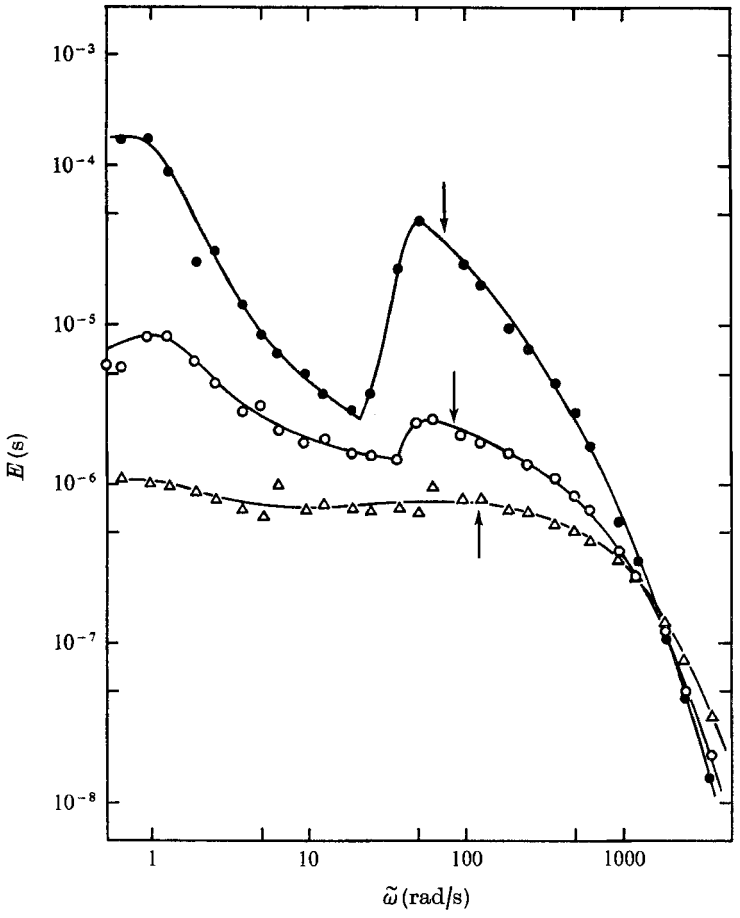

FIGURE 7. Frequency spectrum of a 0·0381 cm diameter local probe in the intermediate turbulent and the turbulent regions. The probe is located at $r = 6{\cdot}01$ cm. The disk speed ω in rad/s is indicated by the arrows. ●, $\omega = 73{\cdot}5$ rad/s, $Re = 2{\cdot}68 \times 10^5$; ○, $\omega = 83{\cdot}2$ rad/s $Re = 3{\cdot}09 \times 10^5$; △, $\omega = 120$ rad/s, $Re = 4{\cdot}46 \times 10^5$.

the outer probe located at 6·01 cm from the disk centre is already out of the transition region and inside the fully developed turbulent region, whereas the inner probe at $r = 4{\cdot}77$ cm is still within the transition region. Again we see an amplification at a frequency corresponding to the rotational speed for the inner probe. The spectrum of the outer probe, on the other hand, is relatively flat; no signs of amplication could be seen within the entire frequency range.

It seems, therefore, that the appearance of an amplification peak is directly related to the existence of stationary vortices. Since the peak frequency always occurs at a frequency approximately equal to that of the disk, it is probable that the size of the stationary vortices is related to the disk frequency. We recall that the wavelength of the stationary vortices in the Ekman boundary layer as found by Faller & Kaylor (1966) is proportional to $(\nu/\omega)^{\frac{1}{2}}$, where ω is the disk frequency. The results of this study agree with their theory that the wavelength of the stationary vortices on the rotating disk is also a function of the rotational speed.

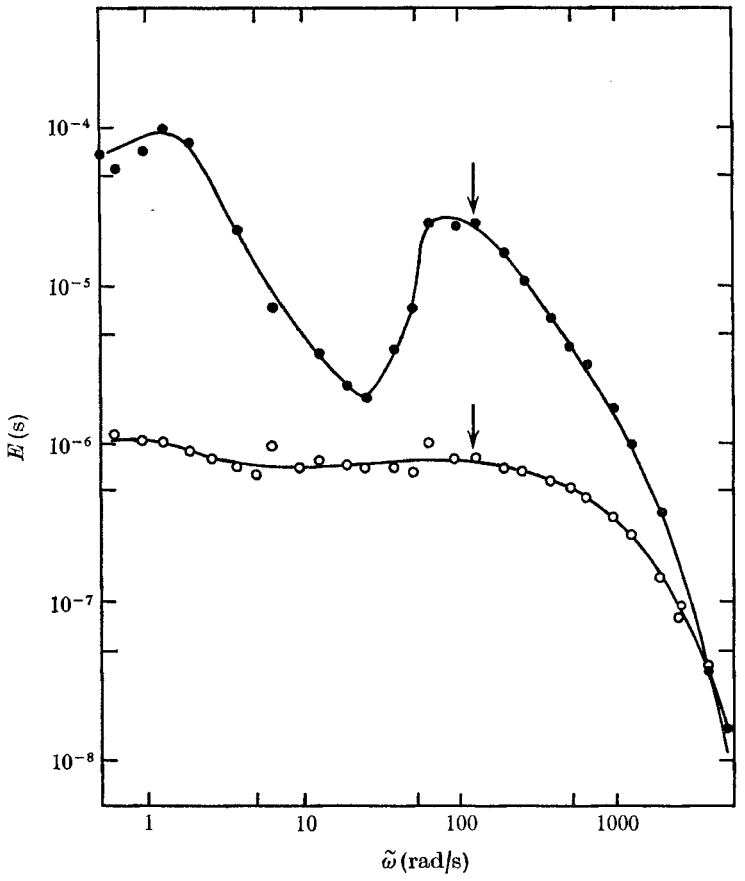

FIGURE 8. Frequency spectrum measured at different radial positions when the disk is rotating at 120 rad/s. A 0·0381 cm diameter local probe is used. The disk speed ω in rad/s is indicated by the arrows. ●, $r = 4{\cdot}77$ cm; $Re = 2{\cdot}72 \times 10^5$; ○, $r = 6{\cdot}01$ cm, $Re = 4{\cdot}46 \times 10^5$.

The frequency spectrum of the tangential probe is similar to that of the local probe, as would be expected from the similarities shown in figure 5. For the radial probe, however, there is no clear amplification of the frequency near the disk speed (Chin 1969); this presumably is due to the inability of the radial probe to detect the stationary vortex.

Also, no conclusion could be drawn from the present data regarding the second mode of instability found in Faller & Kaylor's (1966) experiment. It is apparent that the moving vortices are far away from the disk surface, and cannot be observed using the present technique.

4. Conclusions

On the basis of the above discussion, we may conclude that the electrochemical method gives a more sensitive probe of flow instability than has been possible previously. The transition region on a rotating disk is found to be wider than was thought previously and lies between $Re = 1{\cdot}7 \times 10^5$ and $3{\cdot}5 \times 10^5$. It is

composed of a vortex region ($1{\cdot}7 \times 10^5 < Re < 2{\cdot}6 \times 10^5$), where the intensity of the stationary vortices is found to be increasing with the Reynolds number, and an intermediate turbulent region ($2{\cdot}6 \times 10^5 < Re < 3{\cdot}5 \times 10^5$), where the vortices are breaking down into smaller size eddies. The results of a spectral analysis indicate that the wavelength of the stationary vortices is related to the rotating frequency of the disk.

This work was supported in part by National Science Foundation Grant GK 452.

REFERENCES

BROWN, W. B. 1961 A stability criterion for three-dimensional laminar boundary layers. In *Boundary Layer and Flow Control*, vol. 2 (ed. G. V. Lachmann), pp. 913–923. Pergamon.

CHAM, T. S. & HEAD, M. R. 1969 *J. Fluid Mech.* **37**, 129.

CHIN, D. T. 1969 Ph.D. dissertation, University of Pennsylvania, Philadelphia.

CHIN, D. T. & LITT, M. 1972 Mass transfer to point electrodes on the surface of a rotating disk. *J. Electrochem. Soc.* (in the Press).

COBB, E. C. & SAUNDERS, O. A. 1956 *Proc. Roy. Soc.* A **236**, 343.

FALLER, A. J. & KAYLOR, R. E. 1966 Investigations of stability and transition in rotating boundary layers. In *Dynamics of Fluids and Plasmas* (ed. S. L. Pai *et al.*), pp. 309–329. Academic.

GREGORY, D. P. & RIDDIFORD, A. C. 1960 *J. Electrochem. Soc.* **107**, 950.

GREGORY, N., STUART, J. T. & WALKER, W. S. 1955 *Phil. Trans. Roy. Soc.* A **248**, 155.

GREGORY, N. & WALKER, W. S. 1960 *J. Fluid Mech.* **9**, 255.

HINZE, J. O. 1959 *Turbulence*. McGraw Hill.

JOHNSON, G. R. & TURNER, D. R. 1962 *J. Electrochem. Soc.* **109**, 918.

KEMPF, G. 1924 Über Reibungswiderstand rotierender Scheiben, Vortage auf dem Gebiet der Hydro- und Aerodynamik, *Innsbruck Congr.* 1922, *Berlin.*

KREITH, F., TAYLOR, G. H. & CHONG, J. P. 1959 *J. Heat Transfer, Trans. A.S.M.E.* C **81**, 95.

LEVICH, V. G. 1962 *Physicochemical Hydrodynamics*. Prentice-Hall.

MITCHELL, J. E. & HANRATTY, T. J. 1966 *J. Fluid Mech.* **26**, 199.

REISS, L. P. & HANRATTY, T. J. 1962 *A.I.Ch.E. J.* **8**, 245.

REISS, L. P. & HANRATTY, T. J. 1963 *A.I.Ch.E. J.* **9**, 154.

ROGERS, G. T. & TAYLOR, K. J. 1963*a* *Nature*, **200**, 1062.

ROGERS, G. T. & TAYLOR, K. J. 1963*b* *Electrochem. Acta*, **8**, 887.

SCHMIDT, W. 1921 *Z. ver. dtsch. Ing.* **65**, 441.

SERAD, G. 1964 Ph.D. dissertation, University of Pennsylvania, Philadelphia.

SMITH, H. H. 1947 *N.A.C.A. Tech. Note*, no. 1227.

THEODORSEN, T. & REGIER, A. 1944 *N.A.C.A. Rep.* no. 793.